3D potential field migration for rapid imaging of gravity gradiometry data – A case study from Broken Hill, Australia, with comparison to 3D regularized inversion

Michael S. Zhdanov, University of Utah and TechnoImaging, Xiaojun Liu, University of Utah, Le Wan, Martin Čuma, University of Utah and TechnoImaging, and Glenn A. Wilson, TechnoImaging*

Summary

The geological interpretation of gravity gradiometry data is a very challenging problem. With the exception of the vertical gradient, maps of the different gravity gradients are usually very complicated and cannot be directly correlated with geological structures. We introduce the concept of 3D potential field migration and demonstrate how it can be applied for rapid imaging of entire gravity gradiometry surveys. The method is based on a direct integral transformation of the observed gravity gradients into a 3D density model which can be used for interpretation, or as an a priori model for subsequent 3D regularized inversion. For regional-scale surveys, we show how migration runs on the order of minutes compared to hours for 3D inversion. We present a case study is for the 3D migration of a FALCON® airborne gravity gradiometry (AGG) survey from Broken Hill, Australia, and compare our results to 3D regularized inversion and previously mapped geology.

Introduction

Gravity gradiometry has become widely used in geophysical exploration since it can provide an independent measure of the subsurface density distribution. The advantage of gravity gradiometry over other gravity methods is that the data are extremely sensitive to local density anomalies within regional geological formations. High quality data can be acquired from either airborne or marine platforms over very large areas for relatively low cost. A number of publications have discussed the use of the regularized inversion with both smooth (e.g., Li, 2001) and focusing (e.g., Zhdanov et al., 2004) stabilizers for the interpretation of gravity gradiometry data. A variety of fast imaging techniques related to Euler decomposition have also been developed. Most of these are based on the superposition of analytical responses from specific sources (e.g., Fedi, 2007). These imaging methods typically estimate the positions and some parameters of the sources based on field attenuation characteristics.

In this paper, we present a different approach to imaging based on 3D potential field migration. Migration can be mathematically described as the action of an adjoint operator on observed data. This concept has been long developed for seismic and electromagnetic wavefields (e.g., Schneider, 1978; Berkhout, 1980; Claerbout, 1985; Zhdanov, 1988, 2002, 2009), where the adjoint operators manifest themselves as the (backward) propagation of seismic or electromagnetic fields in reverse time. As applied to potential fields, migration manifests itself as a special form of downward continuation of the potential field and/or its gradients. This downward continuation is applied to the auxiliary field obtained by moving the sources of the true observed field into the upper half-space as the mirror images of the true sources. This transformation results in extrapolation of the field downward and, contrary to conventional downward continuation, away from the mirror images of the sources. Thus migration is a stable transformation similar to conventional upward continuation. As we will demonstrate in this paper, the migration field does contain remnant information about the original source distribution, which is why it can be used for subsurface imaging.

3D potential field migration

Various approximations of the Newton method result in the imaging condition for the vector of densities, $\boldsymbol{\rho}$:

$$\boldsymbol{\rho} = -\lambda^{-1}(\mathbf{W}_m^{-1}\mathbf{W}_m)^{-1}\boldsymbol{l}_0, \quad (1)$$

where λ is the regularization parameter, $\mathbf{W}_m$ is a model weighting matrix, and $\boldsymbol{l}_0$ is the direction of steepest descent (Zhdanov, 2002).

Potential field migration was originally introduced by Zhdanov (2002) and extended to 2D gravity gradiometry by Zhdanov et al. (2010). Here, we briefly describe potential field migration as applied to 3D gravity gradiometry migration. The migration gravity tensor fields, g_α^m, are introduced as a result of applying the adjoint gravity tensor operator, A_α^*, to the observed gravity gradients, g_α:

$$g_{\alpha\beta}^m(\boldsymbol{r}) = A_{\alpha\beta}^* g_{\alpha\beta} = \iint_S \frac{1}{|\mathbf{r}'-\mathbf{r}|^3} g_{\alpha\beta} K_{\alpha\beta}(\boldsymbol{r}'-\boldsymbol{r})ds, \quad (2)$$

where $\alpha, \beta = x, y, z$ and where $K_{\alpha\beta}$ are the respective kernels (i.e., Green's functions) for forward modeling. We can obtain a migration density by substituting equation (2) into equation (1):

$$\rho_{\alpha\beta}^m(\boldsymbol{r}) = -\lambda^{-1}(W_m^{-1}W_m)^{-1}A_{\alpha\beta}^* g_{\alpha\beta}(\boldsymbol{r}), \quad (3)$$

which we can rewrite as follows:

$$\rho_{\alpha\beta}^m(\boldsymbol{r}) = k_{\alpha\beta} w_{\alpha\beta}^2(z) g_{\alpha\beta}^m(\boldsymbol{r}). \quad (4)$$

3D potential field migration for rapid imaging of gravity gradiometry data

The migration fields rapidly attenuate with the depth, as one can see from equation (2). In order to image the sources of the gravity fields at their correct location, one should apply an appropriate spatial weighting operator to the migration fields. This weighting operator, $w_{\alpha\beta}$, is constructed based on the integrated sensitivity of the data to the density, $S_{\alpha\beta}$:

$$w_{\alpha\beta} = \sqrt{S_{\alpha\beta}}. \quad (5)$$

The integrated sensitivity is calculated from the following:

$$S_{\alpha\beta} = c_{\alpha\beta}\frac{1}{z^2}, \quad (6)$$

where $c_{\alpha\beta}$ are the corresponding constants for the different components:

$$c_{zz} = c_{zx} = c_{zy} = \gamma\frac{\sqrt{3\pi}}{2}, c_{xx} = c_{yy} = \gamma\frac{3\sqrt{\pi}}{4}.$$

The unknown coefficient $k_{\alpha\beta} = \lambda^{-1}$ can be determined by linear line search:

$$k_{\alpha\beta} = \frac{\left\|A_{\alpha\beta}^{w*} g_{\alpha\beta}\right\|_M^2}{\left\|A_{\alpha\beta}^{*} A_{\alpha\beta}^{w*} g_{\alpha\beta}\right\|_D^2},$$

where:

$$A_{\alpha\beta}^{w} = A_{\alpha\beta}^{w} W_{\alpha}^{-1}.$$

Equation (4) is called the tensor migration density. It is proportional to the magnitude of the weighted tensor migration fields. Thus, migration provides a stable algorithm for computing the migration density. Substituting equation (6) into equation (4), we find the following:

$$\rho_{\alpha\beta}^{m}(\boldsymbol{r}) = \frac{k_{\alpha\beta}}{c_{\alpha\beta}} z^2 g_{\alpha\beta}^{m}(\boldsymbol{r}). \quad (7)$$

Multiple components can be migrated by linear combination, e.g.,

$$\rho_{\alpha\beta}^{m}(\boldsymbol{r}) = z^2[a_{zz}g_{zz}^{m}(\boldsymbol{r}) + a_{xx}g_{xx}^{m}(\boldsymbol{r}) + a_{\Delta}g_{\Delta}^{m}(\boldsymbol{r})], \quad (8)$$

where $a_{\alpha\beta}$ are weights of the migration fields which may be assigned empirically.

Case study – Broken Hill, Australia

Broken Hill is a historic mining district in New South Wales (NSW), Australia, and host of the world-class Broken Hill stratiform sediment-hosted Ag-Pb-Zn deposit. The host geology consists of the Willyama Supergroup of metamorphosed clastic and volcanoclastic sediments, basic to acid volcanics, and intrusions of 1715 to 1590 Ma age. Mineralization is sediment exhalative in origin and subsequently modified by metamorphism, folding, and shearing (e.g., Parr et al., 2004). Given the significant density contrast between the dense amphibolite- and garnet-altered lithologies and the metamorphosed sedimentary host rocks, gravity methods have been essential in the exploration for Broken Hill-type deposits (e.g., Isles, 1979). Today, mining has virtually eliminated the gravity response of the Broken Hill ore body. Simulations have estimated the maximum g_{zz} response at 80 m ground clearance to be in the range of 10 to 50 Eö over the central lode, similar to the responses of amphibolite units (Lane and Peljo, 2004).

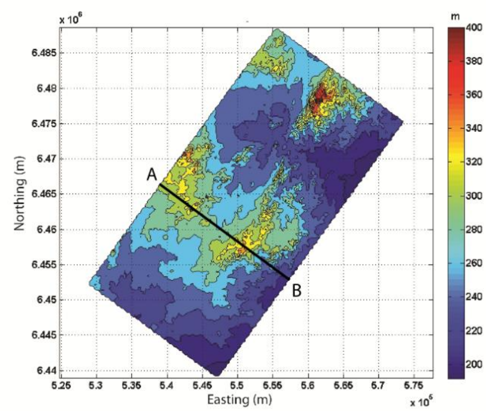

Figure 1. *Topographic relief of the Broken Hill FALCON® survey area. Profile A-B crosses the Broken Hill deposit.*

The FALCON® AGG system measures the horizontal curvature components of the gravity gradient. Other tensor components have been derived from these measured components. In 2003, a 5,600 line km FALCON® airborne gravity gradiometry (AGG) survey was flown in the Broken Hill district to stimulate exploration interest for base metal, Fe-Cu-Au, and Ni-Cu-Pt-Pd deposits (Lane et al., 2003; Lane, 2006). The 44.6 km x 22.5 km survey area was flown at 200 m line spacing approximately parallel to geological strike at 036 degrees (to ensure a maximum sampling rate), with tie lines flown every 2 km. The ground clearance was nominally 80 m flown in a drape over the topographic relief, which varied from 174 m to 421 m above sea level (Figure 1). Hills trend approximately parallel to the flight lines.

3D potential field migration for rapid imaging of gravity gradiometry data

All data were terrain-corrected using a density of 2.75 g/cm^3. This results in a slight positive correlation between the gravity gradients and topography, which is inferred to be acceptable on the grounds that much of the positive topographic relief is comprised of amphibolite- and garnet-altered lithologies that are relatively dense compared to the metamorphosed sediment host rocks that make up the bulk of the survey area (Hensley, 2003). The measured gradients were processed with three processing methods: Fourier domain, equivalent source, and spatial deconvolution. All three processing methods treat noise differently, and as shown in Figure 2, their data ranges and mean variations can be quite significant.

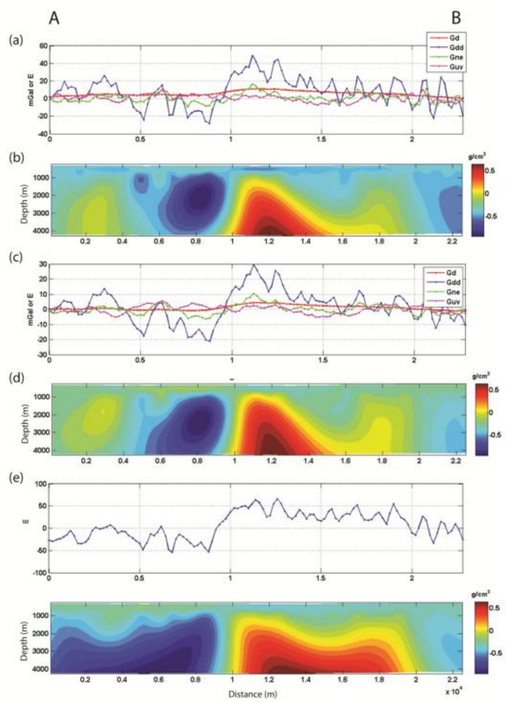

Figure 2. *(a) g_{xy}, g_{Δ}, g_{zz}, and g_z data processed using the Fourier-domain method across profile A-B. (b) Vertical cross section along profile A-B from 3D migration of g_{xy}, g_{Δ}, and g_{zz} data processed using the Fourier-domain method. (c) g_{xy}, g_{Δ}, g_{zz}, and g_z data processed using the equivalent-source method across profile A-B. (d) Vertical cross section along profile A-B from 3D migration of g_{xy}, g_{Δ}, and g_{zz} data processed using the equivalent-source method. (e) g_{zz} data processed using the spatial-deconvolution method across profile A-B. (f) Vertical cross section along profile A-B from 3D migration of g_{zz} data processed using the spatial-deconvolution method.*

With independent results (e.g., 3D regularized inversion), we were able to scale the density contrasts in our 3D migration results. However, for the purpose of rapid 3D imaging, in what follows we select our 3D migration images to vary between density limits of -0.5 and +0.5 g/cm^3. In Figure 2, we show vertical cross sections beneath profile A-B from the 3D density models obtained from 3D migration of data processed by Fourier-domain, equivalent-source and spatial-deconvolution methods. We have also shown the data along profile A-B. Note that there is significant variation in the amplitude of data produced from each data processing method. That said, we note that all 3D migration models show similar features.

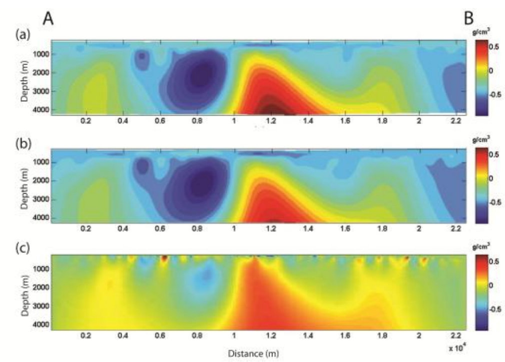

Figure 3. *(a) Vertical cross section along profile A-B from 3D migration of g_{xy}, g_{Δ}, and g_{zz} data processed using the Fourier-domain method. (b) Vertical cross section along profile A-B from 3D migration of g_{zz} data processed using the Fourier-domain method. (c) Vertical cross section along profile A-B from 3D regularized inversion of g_{zz} data processed using the Fourier-domain method.*

We ran our 3D migration jointly for g_{xy}, g_{Δ}, and g_{zz}, as well as singly for g_{zz} only. For this, we considered only the data processed by the Fourier-domain method. For further comparison, we inverted the g_{zz} data using our large-scale 3D regularized inversion (Wilson et al., 2011). The 3D inversion had no a priori model and used focusing regularization. In Figure 3, we show the vertical cross sections beneath profile A-B for the 3D density models obtained from joint 3D migration, 3D migration, and 3D inversion. We note the similarity between the two 3D migration models, and that they are both very similar to the 3D regularized inversion results. As mentioned earlier, the amplitude of the migration results are slightly different from the inversion results because we scaled our migration results to vary between -0.5 and +0.5 g/cm^3. For further comparison of 3D migration and 3D inversion for the g_{zz} data, Figure 4 shows horizontal cross sections at 1000 m depth below topographic peak. Structurally, we observe very good agreement between the models. This agreement is reinforced when we overlay the regional geology, Figure 5. In particular, high-density contrasts are well associated with amphibolites. Moreover, we can image subtle 3D structures, such as the Goldfinger prospect in the southern corner of the survey area.

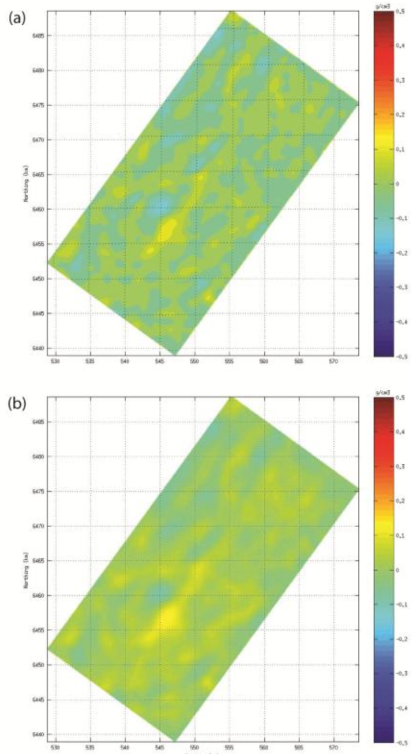

Figure 4. *Horizontal cross sections at -625 m above sea level (~1000 m below topographic peak) from (a) 3D migration of g_{zz} data processed using the Fourier-domain method, and (b) 3D focusing regularized inversion of g_{zz} data processed using the Fourier-domain method.*

Conclusions

We have introduced 3D potential field migration as a new method for rapidly imaging entire surveys of airborne gravity gradiometry (AGG) data. We have shown that potential field migration is an integral transformation of the gravity field and/or its gradients into a unique 3D density distribution. Potential field migration is very fast and stable, and the results are effectively equivalent to those obtained from 3D regularized inversion with smooth stabilizers. 3D migration density models can also be used as a priori models for subsequent 3D regularized inversion with focusing stabilizers. We have demonstrated this with the imaging of nearly 5,000 line km of FALCON® AGG data acquired over the Broken Hill district in Australia. We compared our 3D migration results with those obtained from 3D focusing regularized inversion. We observed very good agreement between those results produced by migration, and those produced by inversion, both of which agree with mapped geology.

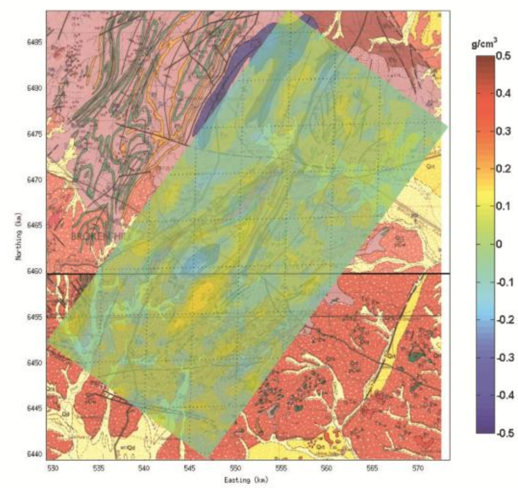

Figure 5. *Horizontal cross section at -625 m above sea level (~1000 m below topographic peak) from 3D migration of g_{zz} data processed using the Fourier-domain method, overlain with the Broken Hill and Menindee 1:250,000 geological maps.*

Acknowledgements

The authors acknowledge TechnoImaging for support of this research, and permission to publish. Zhdanov, Wan, Čuma and Liu acknowledge support of the University of Utah's Consortium for Electromagnetic Modeling and Inversion (CEMI) and Center for High Performance Computing (CHPC). The Broken Hill FALCON® AGG data were made available by the Geological Survey of New South Wales.

EDITED REFERENCES

Note: This reference list is a copy-edited version of the reference list submitted by the author. Reference lists for the 2011 SEG Technical Program Expanded Abstracts have been copy edited so that references provided with the online metadata for each paper will achieve a high degree of linking to cited sources that appear on the Web.

REFERENCES

Berkhout, A. J., 1980, Seismic migration: Elsevier.

Claerbout, J. F., 1985, Imaging the earth's interior: Blackwell Scientific Publications, Oxford.

Fedi, M., 2007, DEXP: A fast method to determine the depth and the structural index of potential fields sources: Geophysics, **72**, I1–I11, doi:10.1190/1.2399452

Hensley, C., 2003, Data processing report, airborne gravity gradiometer survey, Broken Hill, NSW, Australia: BHPBilliton, FALCON Operations Report CR 10657 for Survey USN 142911122002.

Isles, D. J., 1979, A probable extension to the willyama block in N.S.W: Exploration Geophysics, **10**, 191–192, doi:10.1071/EG979191.

Lane, R., 2006, Investigations stemming from the 2003 Broken Hill airborne gravity gradiometer survey, *in* R. J. Korsch, and R. G. Barnes, eds., Broken Hill exploration initiative 2006 conference abstracts, Geoscience Australia Record 2006/21, 116–128.

Lane, R., and M. Peljo, 2004, Estimating the pre-mining gravity and gravity gradient response of the Broken Hill Ag-Pb-Zn deposit: ASEG Extended Abstracts, **1**, 1–5.

Lane, R., P. Milligan, and D. Robson, 2003, An airborne gravity gradiometer survey of Broken Hill, *in* M. Peljo, ed., Broken Hill exploration initiative 2003 conference abstracts, Geoscience Australia Record **2003/13**, 89–92.

Li, Y., 2001, 3-D inversion of gravity gradiometer data: 71st Annual International Meeting, SEG, Expanded Abstracts, 1470-1473, doi:10.1190/1.1816383.

Parr, J. M., B. P. J. Stevens, G. R. Carr, and R. W. Page, 2004, Subseafloor origin for Broken Hill Pb-Zn-Ag mineralization, New South Wales, Australia: Geology, **32**, 589–592.

Schneider, W. A., 1978, Integral formulation for migration in two and three dimensions: Geophysics, **43**, 49–76, doi:10.1190/1.1440828.

Wilson, G. A., M. Čuma, and M. S. Zhdanov, 2011, Massively parallel 3D inversion of gravity and gravity gradiometry data: Preview, in press.

Zhdanov, M. S., 1988, Integral transforms in geophysics: Springer-Verlag.

Zhdanov, M. S., 2002, Geophysical inverse theory and regularization problems: Elsevier.

Zhdanov, M. S., 2009, Geophysical electromagnetic theory and methods: Elsevier.

Zhdanov, M. S., R. Ellis, and S. Mukherjee, 2004, Three-dimensional regularized focusing inversion of gravity gradient tensor component data: Geophysics, **69**, 925–937. doi:10.1190/1.1778236.

Zhdanov, M. S., X. Liu, and G. Wilson, 2010, Potential field migration for rapid 3D imaging of entire gravity gradiometry surveys: First Break, **28**, 47–51, doi:10.3997/1365-2397.2010024.